Multiclass multilane model for freeway traffic mixed with connected automated vehicles and regular human-piloted vehicles

Tianlu Pan[a,b], William H.K. Lam[b], Agachai Sumalee[b], Renxin Zhong[c,b*]

[a]*Research Institute for Smart Cities, School of Architecture and Urban Planning, Shenzhen University, Shenzhen, China.*

[b]*Department of Civil and Environmental Engineering, The Hong Kong Polytechnic University, Hong Kong SAR, China.*

[c]*Guangdong Key Laboratory of Intelligent Transportation Systems, School of Intelligent Systems Engineering, Sun Yat-Sen University, Guangzhou, China*

Abstract: In view of the advantages and a promising market prospect of the emerging connected automated vehicles (CAVs), the number of CAVs will keep increasing rapidly in the coming decade. Meanwhile, the regular human-piloted vehicles (RHVs) may still play a significant role in the roadway traffic. Therefore, it will be very likely that the roadway is shared by CAVs and RHVs in the near future. To support traffic control design, this paper develops a multiclass multilane cell transmission model (CTM) to simulate traffic flow dynamics mixed with CAVs and RHVs by capturing the interaction between the two vehicle classes. First, headway distributions and variations in the fundamental diagram with respect to different penetration rates of CAVs are quantified. Then, the minimum headway acceptance criteria are determined for the lane changing (LC) maneuvers proposed by CAVs and RHVs with consideration on drivers' anticipation. An advanced priority incremental transfer (PIT) principle is then proposed to evaluate the sending flows. Finally, the cell-lane-specific multiclass flow conservation law is developed to propagate traffic flow and density considering the vehicle LC maneuvers. Numerical simulations explore the potential operational capacity increase, delay reduction, and traffic flow smoothing under several penetration scenarios.

Keywords: Vehicle Automation and Communication System (VACS); Multiclass multilane cell transmission model; Connected automated vehicle (CAV); Penetration rate; Capacity variation.

1 Introduction

The advancement of cyber-physical systems enables vehicles to form a mobile wireless network on the road called vehicular ad hoc network (VANET), which links vehicles with roadway infrastructures via wireless communication. As a promising technology, VANET offers the following two types of communications: vehicle-to-vehicle (V2V) and vehicle-to-infrastructure (V2I). In view of the promising market prospect, enormous efforts have been exerted by the automobile industry and numerous institutions toward the development, testing, and deployment of Vehicle Automation and Communication Systems (VACS) in recent years because they are believed to bring benefits to traffic safety and efficiency (Diakaki et al., 2015). For example, through the aid of VACS, an effective approach is to change the driving behavior from individual car following (CF) to a platoon-

* Corresponding author: R. X. ZHONG, *E-mail address:* zhrenxin@mail.sysu.edu.cn (R. X. ZHONG).

The work described in this paper is part of the PhD research work of T. Pan conducted at the Hong Kong Polytechnic University.

based driving, that is, a cooperative driving pattern for a group of vehicles wherein a vehicle follows the preceding vehicle with a small and nearly constant safety space/time headway to form platoons (Ngoduy and Jia, 2016). The literature has validated that the platoon-based driving pattern with fully automated vehicles can significantly improve roadway capacity and introduce numerous benefits (Hall and Chin, 2005; van Arem et al., 2006). A recent experiment at the California Partners for Advanced Transit and Highways (PATH) showed that connected automated vehicles (CAVs) in platoons could maintain a time gap as small as 0.6 sec compared with 1.5 sec for regular human-piloted vehicles, thereby possibly nearly doubling the roadway capacity (Chen et al., 2017).

The reduced reaction time of CAVs can improve traffic flow efficiency via smaller inter-vehicle headway (Levin and Boyles, 2016a; Zhou et al., 2017; Zhu and Ukkusuri, 2017). Stern et al. (2018) demonstrated in the mixed-autonomy single-lane ring road experiments (consisting of 22 RHVs on a 230m ring track) that a reduction in fuel consumption over 40% can be achieved by the insertion of a CAV in the traffic to dampen the ring instability. Given that vehicle platooning can significantly reduce the air drag of vehicles inside the platoon, energy consumption and exhaust emissions can also be considerably reduced as a result. The cooperative driving pattern of CAVs can increase roadway capacity to double (or higher) and can significantly improve traffic flow stability (Milanes et al., 2014; Milanes and Shladover, 2014). Talebpour and Mahmassani (2016) proposed a framework to simulate traffic flow characteristics consisting of CAVs with distinct communication capabilities and RHVs under certain technology-appropriate assumptions. It was shown numerically that the CAVs can improve string stability and be more effective in preventing shockwave formation and propagation.

As it can be expected, the number of connected automated vehicles (CAVs) equipped with VACS will be rapidly increasing in the coming decade. Meanwhile, the regular human-piloted vehicles (RHVs) still play a major role in the market in the short term (Levin and Boyles, 2016a,b). Therefore, it will be common that the road is shared by CAVs and RHVs in the near future. To the best of the authors' knowledge, most efforts have adopted simulations, whereas limited theoretical research has been conducted. The mechanism on **how the CAVs help improve the operational capacity is unclear due to the complicated (car following) CF and LC rules** specified in the simulations. Nevertheless, **systematic investigation of the influences of CAVs on collective (macroscopic) traffic flow and sustainability remains insufficient** (Khondaker et al., 2015; Wang et al., 2015, 2016a,b). All these factors impede the development of trusted and fast traffic flow models for Active Traffic Management for traffic flow mixed with CAVs and RHVs. Thus, research and development activities can be further developed.

Under the car-following framework, Jia and Ngoduy (2016b) developed a microscopic traffic model that simulates the cooperative driving behavior in terms of platooning via inter-vehicle communication. An enhanced cooperative microscopic car-following traffic model was proposed in Jia and Ngoduy (2016a) to consider how V2V and V2I communications affect the vehicle cooperative driving, e.g., the local traffic flow stability and shock wave smoothing. Zhu and Ukkusuri (2017a) proposed a cell-based simulation approach to simulate the proactive driving behavior of CAVs by tracking the trajectory of CAVs and adjusting the exit flow of cells containing connected vehicles. To study the car-following behavior of CAVs following RHVs, Zhu and Ukkusuri (2017b)

developed an approach to calibrate CAVs' car following behavior in a mixed traffic environment using the simplified car-following model with disturbances. Zhou et al. (2017) developed a cooperative intelligent driver model to examine the system performance of freeway merging under different proportions of CAVs. Jia et al. (inpress) proposed a multiclass microscopic model that includes a consensus-based control algorithm to model the dynamics of CAVs and a car-following model to describe the dynamics of RHVs.

The average speed of RHVs is approximately equal to the average speed of connected vehicles in a traffic stream (Bekiaris-Liberis et al., 2016; Fountoulakis et al., 2017). Based on scalar conservation law, Bekiaris-Liberis et al. (2016) proposed a Kalman filter approach to estimate the density and flow for traffic comprising regular and connected vehicles using the average speed measurements from connected vehicles and spot-sensor-based total flow measurements. Fountoulakis et al. (2017) further investigated this estimation approach through microscopic simulation while revealing different CF behaviors between these two vehicle classes. Wang et al. (2017) extended the second-order traffic flow model and modeled traffic streams with mixed RHVs and CAVs. Based on the model, the traffic state is estimated via a nonlinear particle filtering approach. Roncoli et al. (2015), Levin and Boyles (2016a,b) extended the CTM to simulate the mixed traffic flow with regular and connected vehicles. **The existing multiclass CTM models modified the fundamental diagram to consider the variations in capacity and backward wave speed in response to vehicle-class proportions within each cell while LC maneuvers were not considered.** Chen et al. (2017) proposed traffic operational capacity formulations for mixed traffic under equilibrium. They found that a macroscopic capacity can be properly identified for the mixed traffic by considering the proportion of CAVs, the micro/mesoscopic characteristics of the two vehicle classes, and different lane policies.

As reviewed in this section, a **rather limited research effort** has been dedicated to addressing **the implications of the emerging VACS on the flow characteristics of traffic mixed with RHVs and CAVs, as well as their potential exploitation for improving traffic flow operations** (Diakaki et al., 2015). All these impede the development of trusted and fast traffic flow models for ATM of traffic flow mixed with CAVs and RHVs. To simulate the traffic flow characteristics and to support the integrated freeway traffic control design and subsequently improve the performance efficiency of freeways, this study intends to develop a multilane traffic flow model to simulate traffic flow dynamics mixed with CAVs and RHVs. The main contributions of this paper are twofold:

a) We propose a multiclass multilane macroscopic model to explore the interaction between RHVs and CAVs. The model is capable of evaluating the variations in the fundamental diagrams with respect to the penetration rate of CAVs.
b) The model develops a set of minimum headway acceptance criteria for LC maneuvers of RHVs and CAVs; The model simulates the **LC maneuvers of both vehicle classes** while considering drivers' anticipation.

Pan et al. (2016) developed a multilane CTM to simulate the impacts of MLC and DLC maneuvers on traffic flow comprised of RHVs. As reviewed, several factors, e.g., the uncertain penetration rate of CAVs, human drivers' behavior, and lane-changing maneuvers, affect the characteristics of traffic flow with mixed RHVs and CAVs. In this paper, the multilane cell transmission model (CTM) proposed by Pan et al. (2016) is extended from a single vehicle class to multiple vehicle classes to

consider the factors mentioned above. To be specific, we extend this model to multiclass traffic by incorporating several new features: (1) modeling the time-dependent proportion of CAVs on the cell-lane traffic flow characteristics such as the lane-based fundamental diagram and vehicle-class-specific minimum space headway acceptance criteria to guarantee the traffic safety and lane-changing priorities; (2) simulating lane-changing maneuvers considering lane-changing priorities with respect to different vehicle classes and the lane-changing motivations; and (3) extending new sending and receiving functions governing flow propagation considering the lane-changing flows and multiclass cell-lane fundamental diagrams.

It is assumed in this paper that the V2X communication is always reliable and the control issued to the CAVs can be well actuated. The CAVs know the position and speed of some following vehicles and the direct preceding vehicle in real time regardless whether the following and the preceding vehicles are CAVs or not using either through V2X technology or via their own detector (Jia and Ngoduy, 2016a; Lioris et al., 2017).

The rest of the paper is organized as: Section 2 presents the traffic flow characteristic mixed with CAVs and RHVs. Section 3 presents the traffic flow propagation under the lane-based multiclass CTM framework. Numerical simulations are conducted in Section 4 to demonstrate the effects of CAVs on speed, operational capacity, travel time and different penetration rates of CAVs. Section 5 concludes the paper. Notation list and companion materials are provided in the Appendix.

2. The multiclass traffic flow characteristics mixed with CAVs and RHVs

As reviewed in Section 1, several factors, e.g., the uncertain penetration rate of CAVs, human drivers' behavior, and lane-changing maneuvers, affect the characteristics of traffic flow with mixed RHVs and CAVs. In this section, the multilane cell transmission model (CTM) proposed by Pan et al. (2016) is extended from a single vehicle class to multiple vehicle classes.

2.1. Headway distribution and fundamental diagram

Headway, defined as the time/space between the same positions of two consecutive vehicles, is an important measure of traffic flow characteristics, and thus it is essential for studying traffic flow. Because CAVs have significantly different operating characteristics compared to RHVs, e.g., ignorable reaction time and platooning, it is deemed that CAVs can significantly reduce the headway between vehicles and hence increase the roadway capacity (Levin and Boyles, 2016b; Chen et al., 2017). Therefore, it is necessary to define a headway distribution law to model the capacity enhancement with the introduction of CAVs and to enable minimum headway control for the mixed traffic.

In line with Levin and Boyles (2016b) and Chen et al. (2017), the effect of CAVs on roadway capacity was investigated by considering a single-lane freeway segment, as depicted in Figure 1. Suppose a platoon of vehicles is traveling along a freeway section in the same lane and that the traffic flow is stable without interruption from on-ramp/off-ramp or traffic incidents. Based on the

rear-end collision avoidance principle (Jepsen, 1998; Levin and Boyles, 2016b), for vehicles traveling at speed $v(t)$ (miles/hour) the space headway (from the head of the leading vehicle to the head of the following vehicle) criterion $H_D(t)$ (mile) ahead of a specific vehicle belongs to vehicle class D is defined as below:

$$H_D(t) \geq v(t)\Delta T_D + l + C, \quad for\ D = CAV, RHV \tag{1}$$

where ΔT_{CAV} and ΔT_{RHV} (hour) denote the response times of CAVs and RHVs, respectively, l (mile) denotes the vehicle length of the leading vehicle, and C is the safety gap (Jepsen, 1998) or minimum safe constant gap (Hidas, 2005) when all the vehicles are at a standstill. Compared with RHVs, CAVs can tolerate a much smaller space headway because of the smaller response time. Supposing that the traffic on this unit length freeway segment (otherwise, multiply both sides of Equation **Error! Reference source not found.** by the segment length) with a proportion, $P(t)$, of CAVs and RHVs, 1-$P(t)$, at time t, the relationship between space headway and traffic density is described as

$$\rho(t)\left(P(t)H_{CAV}(t) + \left(1 - P(t)\right)H_{RHV}(t)\right) = 1 \tag{2}$$

where $\rho(t)$ is the traffic density, $H_{CAV}(t)$ and $H_{RHV}(t)$ denote the space headway of CAVs and RHVs, respectively, as illustrated in Figure 1.

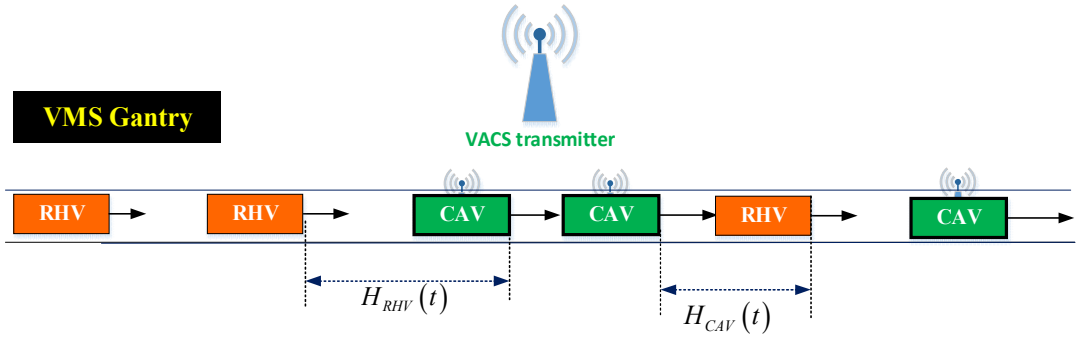

Figure 1 Illustration of space headway of mixed freeway traffic

Based on Equation **Error! Reference source not found.**, we have the following relations:

$$\rho(t)P(t)H_{CAV}(t) \geq \rho(t)P(t)\left(v(t)\Delta T_{CAV} + l + C\right)$$
$$\rho(t)\left(1 - P(t)\right)H_{RHV}(t) \geq \rho(t)\left(1 - P(t)\right)\left(v(t)\Delta T_{RHV} + l + C\right)$$

Summing the left and right sides, respectively, we obtain

$$\rho(t)\left(P(t)H_{CAV}(t) + \left(1 - P(t)\right)H_{RHV}(t)\right)$$
$$\geq \rho(t)P(t)\left(v(t)\Delta T_{CAV} + l + C\right) + \rho(t)\left(1 - P(t)\right)\left(v(t)\Delta T_{RHV} + l + C\right)$$

This in conjunction with Equation **Error! Reference source not found.** provides

$$1 \geq \rho(t)P(t)\left(v(t)\Delta T_{CAV} + l + C\right) + \rho(t)\left(1 - P(t)\right)\left(v(t)\Delta T_{RHV} + l + C\right)$$

Therefore, the maximum speed $\tilde{v}_s(t)$ that can be evaluated by specific traffic density and proportion

of CAVs is evaluated as follows:

$$\tilde{v}_s(t)=\frac{\left(1-l\cdot\rho(t)-C\cdot\rho(t)\right)}{\rho(t)}\cdot\frac{1}{\left(P(t)\ \Delta T_{CAV}\ +\left(1-P(t)\right)\ \Delta T_{RHV}\right)} \tag{3}$$

without considering the speed limit or vehicles' mechanical capability. As reported in the literature, the average speed of RHVs is roughly equal to the average speed of CAVs in a traffic stream (Bekiaris-Liberis et al., 2016; Fountoulakis et al., 2017). To this end, it is assumed that both CAVs and RHVs will spontaneously follow this maximum speed as it guarantees the minimum space gap for avoiding collisions in accordance with different levels of congestion specified by traffic density. Therefore, in this section, the variable $\tilde{v}_s(t)$ is named the **spontaneous speed limit** (SSL). However, when the traffic density tends to zero (i.e., no vehicle is traveling on the freeway), the SSL approaches an infinitely large value. To remedy this, one can simply set an upper bound to this SSL, called a vehicle's **maximum mechanical speed**. For example, 170 miles/hour is a typical upper bound of the speedometer of private vehicles. Generally speaking, the speed is actually restricted by the posted **permanent compulsory** (upper bound) **speed limit** for freeway traffic management purpose. In the United States under normal conditions, the posted permanent compulsory freeway speed limit ranges from 90 miles/hour in rural areas to 40 miles/hour in urban areas (Highway Capacity Manual, 2010). Additionally, a temporary VSL can be issued as a control strategy for traffic incident management or congestion resolution if needed. As it can be expected, **maximum mechanical speed > permanent compulsory speed limit > temporary VSL**; therefore, the **implemented speed limit (ISL)** is generally given as either the permanent compulsory speed limit or the temporary VSL.

In line with the VSL control literature, e.g., Hegyi et al. (2005), the turning point of ISL and SSL is located at the critical density $\rho_c(t)$ (noting that the critical density is also affected by the implemented speed limited control itself), as shown in Figure 2. From the above analysis, the traffic flow speed $v(t)$ is finally defined as a function of ISL (the lower of the posted compulsory speed limit and the VSL), traffic density, and the proportion of CAVs.

$$v(t)=\begin{cases}\tilde{v}_l(t) & \text{if } \rho(t)\le\rho_c(t)\\ \tilde{v}_s(t)=\dfrac{\left(1-l\cdot\rho(t)-C\cdot\rho(t)\right)}{\rho(t)}\cdot\dfrac{1}{\left(P(t)\ \Delta T_{CAV}\ +\left(1-P(t)\right)\ \Delta T_{RHV}\right)} & \text{if } \rho(t)>\rho_c(t)\end{cases} \tag{4}$$

where $\tilde{v}_l(t)$ denotes the ISL (which can be regarded as a decision variable of the dynamic optimization problem as discussed in our recent work Pan et al. (preprint) or the permanent compulsory speed limit posted by freeway management center) and $\rho_c(t)$ is a function of the penetration rate of CAVs and ISL as follows:

$$\rho_c(t)=\frac{1}{\tilde{v}_l(t)\left(P(t)\ \Delta T_{CAV}\ +\left(1-P(t)\right)\ \Delta T_{RHV}\right)+l+C} \tag{5}$$

In traffic flow theory, the flow is the product of speed, $v(t)$, and density, $\rho(t)$, whereas the capacity

is the maximum traffic flow (rate) observed at the critical density $\rho_c(t)$. By $Q_m(t)=\rho_c(t)\tilde{v}_l(t)$, the roadway capacity can be defined below as a function of the penetration rate of CAVs and ISL:

$$Q_m(t)=\frac{\tilde{v}_l(t)}{\tilde{v}_l(t)\left(P(t)\ \Delta T_{CAV}\ +\left(1-P(t)\right)\ \Delta T_{RHV}\right)+l+C} \tag{6}$$

For the congested part, according to Equation (4), the flow can be evaluated as

$$\rho(t)\tilde{v}_s(t)=\rho(t)\frac{\left(1-l\cdot\rho(t)-C\cdot\rho(t)\right)}{\rho(t)}\cdot\frac{1}{\left(P(t)\ \Delta T_{CAV}\ +\left(1-P(t)\right)\ \Delta T_{RHV}\right)}$$
$$=\frac{1-(l+C)\rho(t)}{\left(P(t)\ \Delta T_{CAV}\ +\left(1-P(t)\right)\ \Delta T_{RHV}\right)}$$

Assuming a linear relationship in the congested part, we have

$$w_c(t)\left(\rho_J-\rho(t)\right)=w_c(t)\left(\frac{1}{l+C}-\rho(t)\right)=\frac{1-(l+C)\rho(t)}{\left(P(t)\ \Delta T_{CAV}\ +\left(1-P(t)\right)\ \Delta T_{RHV}\right)}$$
$$=\frac{l+C}{\left(P(t)\ \Delta T_{CAV}\ +\left(1-P(t)\right)\ \Delta T_{RHV}\right)}\left(\frac{1}{l+C}-\rho(t)\right)$$

Therefore the back-wave speed is evaluated by:

$$w_c(t)=\frac{l+C}{\left(P(t)\ \Delta T_{CAV}\ +\left(1-P(t)\right)\ \Delta T_{RHV}\right)} \tag{7}$$

while the jam density is determined by the average vehicle length and the minimum safe constant gap:

$$\rho_J=\frac{1}{l+C} \tag{8}$$

To ensure safety, the minimum space headway criteria $\tilde{H}_D(t)$ for vehicle class *D = CAV and RHV* are evaluated respectively as

$$\begin{aligned}\tilde{H}_{CAV}(t)&=v(t)\Delta T_{CAV}+l+C\\ \tilde{H}_{RHV}(t)&=v(t)\Delta T_{RHV}+l+C\end{aligned} \tag{9}$$

The total space $\tilde{O}(t)$ reserved for the minimum-space headway of all vehicles traveling on the freeway segment is calculated according to the proportions of the two vehicle classes.

$$\tilde{O}(t)=\rho(t)P(t)\tilde{H}_{CAV}(t)+\rho(t)\left(1-P(t)\right)\tilde{H}_{RHV}(t) \tag{10}$$

When $\rho(t)\geq\rho_c(t)$, the speed is determined by SSL $\tilde{v}_s(t)$ according to Equation (4), the total space $\tilde{O}(t)$ reserved for the minimum-space headways fills the total spaces. That is, the relationship between the traffic speed and density attains a critical value, as illustrated in **Error! Reference source not found.**2. The flow speed cannot be increased so as to maintain safety. However, when

$\rho(t)<\rho_c(t)$, ISL $\tilde{v}_l(t)$ can be lower than SSL $\tilde{v}_s(t)$, thus allowing extra space.

$$\tilde{O}(t)\begin{cases}<1 & if\ \rho(t)<\rho_c(t)\\ =1 & if\ \rho(t)\geq\rho_c(t)\end{cases}$$

That is to say, if there is no ISL $\tilde{v}_l(t)$, vehicles can travel faster under light traffic conditions. The free space 1-$\tilde{O}(t)$ not occupied by vehicles can be randomly distributed among them. For simplification, we assume the safe space headway criteria are magnified by $\frac{1}{\tilde{O}(t)}$, i.e.,

$$\begin{aligned}H_{CAV}(t)&=\tilde{H}_{CAV}(t)/\tilde{O}(t)\\ H_{RHV}(t)&=\tilde{H}_{RHV}(t)/\tilde{O}(t)\end{aligned}\qquad if\ \rho(t)<\rho_c(t)$$

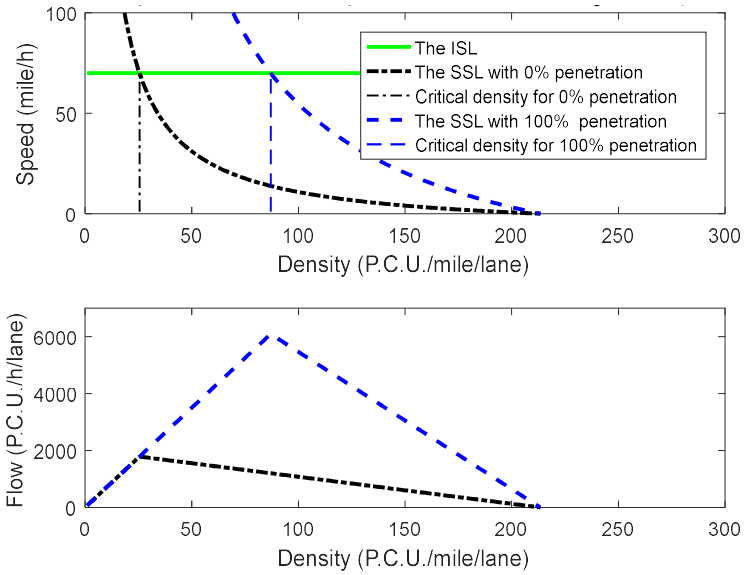

Figure 2 Lane-specific fundamental diagram as a function of the penetration rate of CAVs.

To sum up, the (average) space headway distributions are thus calculated:

$$H_{CAV}(t)=\begin{cases}\dfrac{v(t)\Delta T_{CAV}+l+C}{\rho(t)\cdot(l+C)+\rho(t)\cdot v(t)\cdot\left(P(t)\ \Delta T_{CAV}+(1-P(t))\ \Delta T_{RHV}\right)} & if\ \rho(t)<\rho_c(t)\\ v(t)\cdot\Delta T_{CAV}+l+C & if\ \rho(t)\geq\rho_c(t)\end{cases}$$

$$H_{RHV}(t)=\begin{cases}\dfrac{v(t)\Delta T_{RHV}+l+C}{\rho(t)\cdot(l+C)+\rho(t)\cdot v(t)\cdot\left(P(t)\ \Delta T_{CAV}+(1-P(t))\ \Delta T_{RHV}\right)} & if\ \rho(t)<\rho_c(t)\\ v(t)\cdot\Delta T_{RHV}+l+C & if\ \rho(t)\geq\rho_c(t)\end{cases}\qquad(11)$$

As stated in Green (2000), the brake response time of a human driver is composed of three

components: mental processing, muscle movement, and brake engagement time. On average, the mental processing takes about 1.3 sec for unexpected occasions, the average muscle movement takes 0.2 sec (Wierwille and Casali, 1983; Lerner et al., 1995; Green 2000), and the brake engagement time takes 0.35 sec under emergency conditions. Therefore, the braking response time of RHVs to an unexpected occasion is 1.85 sec. However, CAVs do not have mental reactions nor muscle movement; therefore, the response time of CAVs is considered to be 0.35 sec for the brake engagement process. This value is consistent with the 0.6 sec time headway between successive CAVs (Chen et al., 2017).

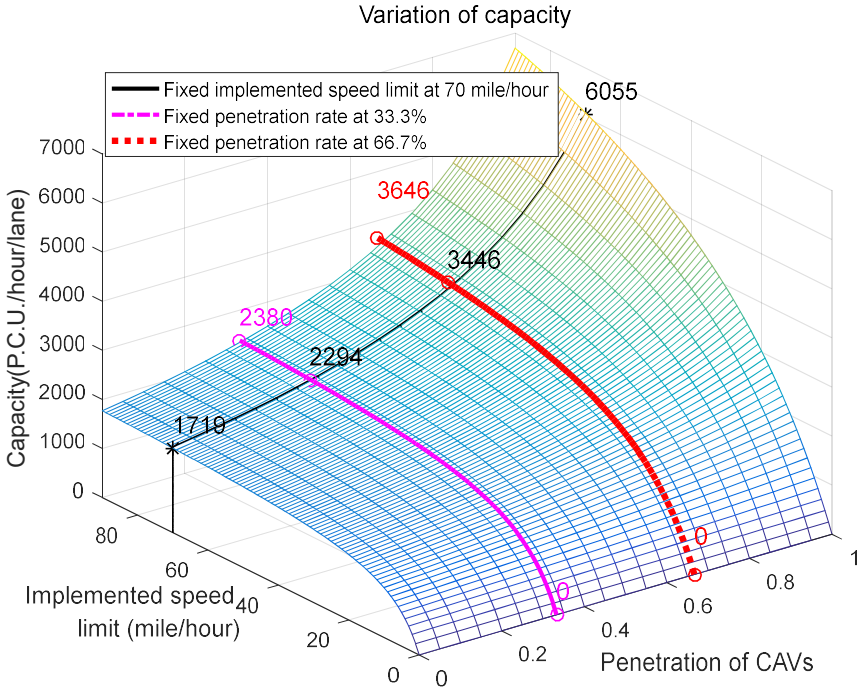

Figure 3 Capacity as a function of the penetration rate of CAVs and implemented speed limit.

Figure 3 demonstrates the impact of the penetration rate of CAVs[1] and the compulsory speed limit on road capacity. In this example, all vehicles are considered passenger car equivalent (P.C.E.) or passenger car unit (P.C.U.) vehicles 20 ft in length, and the safe constant gap is 6.5 ft (when the related vehicles are at a standstill). As stated above, the response times of RHVs and CAVs are set to be 1.85 sec and 0.35 sec, respectively. As shown in Figure 3, the capacity monotonically increased with the increasing penetration rate of CAVs and the ISL. The solid black line quantifies the variation of capacity with respect to the penetration rate of CAVs varying from 0% to 100% by fixing the compulsory speed limit at 70 miles/hour. As demonstrated in this figure, the capacity varies significantly from 1719 P.C.U./hour/lane (with 100% RHVs) to 6055 P.C.U./hour/lane (with 100% CAVs). On the other hand, by conventional macroscopic traffic flow theory, the increase in free-flow speed (or the compulsory speed limit in our case) would introduce an increase in capacity. The red dotted line presents an example for this using a fixed 66.7% penetration rate of CAVs, while the pink dot-dash line presents the 33.3% one.

[1] In this case, the penetration rate is equivalent to proportion as we interest in cell-lane capacity.

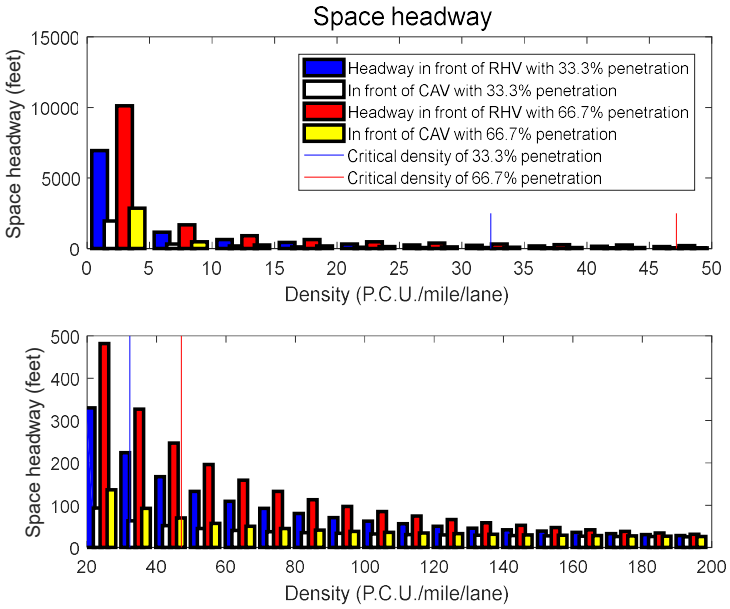

Figure 4 The distribution of space headway as a function of the penetration rate of CAVs

Table 1 Space headway as a function of traffic density and penetration rate of CAVs

	Scenario: 33.3% Penetration rate			Scenario: 66.7% Penetration rate		
Density (P.C.U./mile/ lane)	Speed (miles/hour)	$H_{CAV}(t)$ (ft)	$H_{RHV}(t)$ (ft)	Speed (miles/hour)	$H_{CAV}(t)$ (ft)	$H_{RHV}(t)$ (ft)
10	**70**	**196**	**694**	**70**	**286**	**1012**
32	**70**	**61**	**217**	**70**	**89**	**316**
47	49	47	145	**70**	**61**	**215**
100	14	32	63	20	36	86
200	0.8	25	27	1	25	28

Figure 4 and Table 1 present the space headways of RHVs and CAVs with respect to traffic density and penetration of CAVs. The space headway distributions with respect to different penetration rates of CAVs depicted in Figure 5 were obtained by setting the traffic density to be 47 P.C.U./mile/lane, i.e., 3 P.C.U./337ft, and assuming 66.7% and 33.3% penetration rates of CAVs, respectively. As it can be inferred from Figure 4, 5 and Table 1 that:

1) The space headway in front of an RHV is larger than that in front of a CAV under the same traffic conditions, and this difference is more significant under free-flowing conditions (the results related to free-flowing conditions use bold font in Table 1).

2) The increment of traffic density leads to smaller space headways for both RHVs and CAVs.

3) The penetration rate of CAVs affects the space headway distribution. In particular, the space headway in front of RHVs increases when the penetration rate of CAVs raises from 33.3% to 66.7%.

4). With the same traffic density, the traffic with a higher penetration rate of CAVs might maintain a higher speed. As demonstrated in Figure 5, the traffic is 21 miles/hour faster when the penetration rate of CAVs raises from 33.3% to 66.7%.

As it can be inferred from the above observations, the introduction of CAVs can change the gap distribution of the target lanes, while this change makes the lane changing maneuvers easier to be accepted by the target lanes.

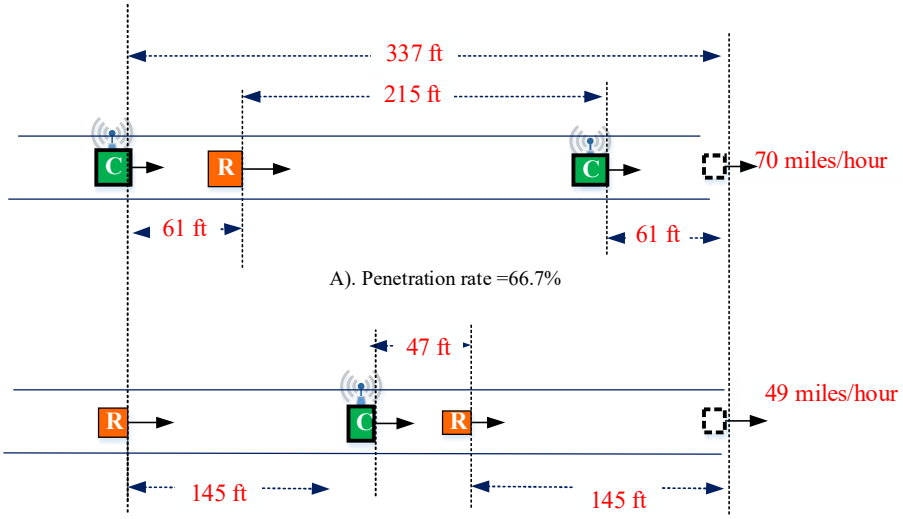

Figure 5 The variation of space headway with respect to penetration rate.

2.2. The minimum gap acceptance criteria

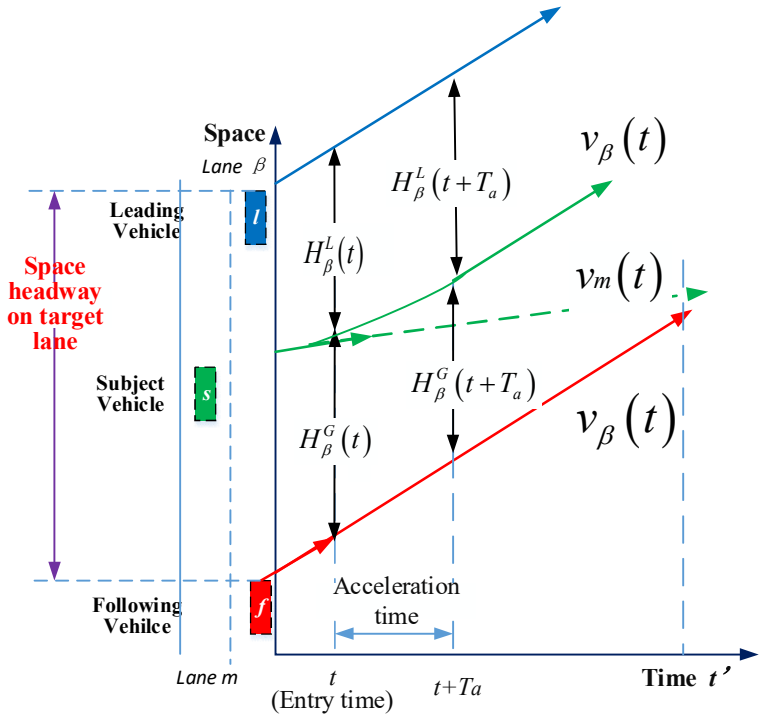

Figure 6 The headway acceptance analysis

Apart from the traffic flow characteristics associated with traffic flow on a single lane, such as in the fundamental diagram and space headway distribution introduced in Section 2.1, the penetration

of CAVs also has an impact on lane-changing maneuvers when traveling on multilane freeways. In this subsection, the lane-changing acceptance/rejection criteria for multiclass traffic is proposed by extending the counterparts from Pan et al. (2016).

Suppose that the subject vehicle s traveling on lane m switches to lane β via the space gap between the leading vehicle l and the following vehicle f in the target lane at time t, as demonstrated in Figure 6. It is assumed that the subject vehicle is traveling at speed $v_m(t)$ (miles/hour), whereas the leading vehicle and following vehicle in the target lane are both traveling at the same speed $v_\beta(t)$ (miles/hour). Without loss of generality, the assumption $v_m(t) < v_\beta(t)$ is proposed in this section, i.e., the lane-changing maneuver is executed to gain better driving conditions. Based on the speed difference assumption $v_m(t) < v_\beta(t)$, it is necessary for the subject vehicle to accelerate to avoid a collision with the following vehicle in the target lane after the lane changing maneuver is executed. During the acceleration process, the space gap between the leading vehicle and the following vehicle must always fulfill the collision avoidance criteria. Denoting $t' = t + T_a$ (*hour*) as the moment when the lane-changing maneuver is executed, as shown in Figure 6, the subject vehicle is supposed to travel at the same speed as the vehicles in the target lane. By assumption, this speed is $v_m(t+T_a)=v_\beta(t+T_a)=v_\beta(t)$. Considering the speed difference between the related vehicles during the lane-changing maneuver, the leading space headway[2] $H_\beta^L(t')$ (mile) (as shown in Figure 6) will gradually increase, whereas the lag space headway $H_\beta^G(t')$ (mile) will decrease with respect to the acceleration and lane-changing maneuver of the subject vehicle, that is,

$$\begin{cases} H_\beta^L(t')=H_\beta^L(t)+\left(v_\beta(t)-v_m(t)\right)\cdot(t'-t)-\dfrac{1}{2}a\cdot(t'-t)^2 \\ H_\beta^G(t')=H_\beta^G(t)-\left(v_\beta(t)-v_m(t)\right)\cdot(t'-t)+\dfrac{1}{2}a\cdot(t'-t)^2 \end{cases} \quad for\ \ t\le\forall t'\le t+T_a \tag{12}$$

and

$$\begin{cases} H_\beta^L(t')=H_\beta^L(t+T_a) \\ H_\beta^G(t')=H_\beta^G(t+T_a) \end{cases} \quad for\ t'>t+T_a$$

According to the collision avoidance principle described in Section 2.1, the following conditions need to be fulfilled:

$$\begin{cases} H_\beta^L(t')\ge\left(v_m(t)+a\cdot(t'-t)\right)\Delta T_{D,\,s}+l+C \\ H_\beta^G(t')\ge v_\beta(t)\Delta T_{D,\,f}+l+C \end{cases} \quad for\ t\le\forall t'\le t+T_a \tag{13}$$

where $\Delta T_{D,\,s}$ and $\Delta T_{D,\,f}$ denote the response times of the subject and the following vehicles,

[2]The leading space headway denotes the distance from the head of the lead vehicle to the head of the subject vehicle. The lag headway denotes the distance from the head of the subject vehicle to the head of the following vehicle.

respectively. The space headway of the target lane at time t, $H_{s,m}^{f,\beta}(t)=H_{\beta}^{L}(t)+H_{\beta}^{G}(t)$, should be not less than the minimum space headway $\tilde{H}_{s,m}^{f,\beta}(t)$, which is determined by Equation (14):

$$H_{s,m}^{f,\beta}(t)\geq\tilde{H}_{s,m}^{f,\beta}(t)=\begin{cases}\left[\underbrace{v_{\beta}(t)\Delta T_{D,f}}_{item\,1}+\underbrace{v_{m}(t)\Delta T_{D,s}}_{item\,2}+\underbrace{\frac{\left(v_{\beta}(t)-v_{m}(t)\right)^{2}}{2a}}_{item\,3}\right]+\underbrace{(2l+2C)}_{item\,4} & Case\,1\\ \left[\underbrace{v_{\beta}(t)\Delta T_{D,f}}_{item\,1}+\underbrace{v_{m}(t)\Delta T_{D,s}}_{item\,2}+\underbrace{\frac{\left(v_{\beta}(t)-v_{m}(t)\right)^{2}}{2a}}_{item\,3}\right]\frac{x-x_{c}}{x_{r}-x_{c}}+\underbrace{(2l+2C)}_{item\,4} & Case\,2\\ \underbrace{(2l+2C)}_{item\,4} & Case\,3\end{cases} \quad (14)$$

This criterion varies with respect to the lane-changing motivation, level of lane-changing urgency, and vehicle class. According to the level of urgency, $\tilde{H}_{s,m}^{f,\beta}(t)$ is divided into three cases. Case 1 refers to the non-urgent scenario associated with a lane-changing demand proposed by RHVs, such as a discretionary demand or a mandatory demand at a remote state with the remaining distance[3] $x>x_r$. Under this case, drivers usually prefer a relatively large gap at the beginning of a lane-changing maneuver due to a risk-adverse attitude. $\tilde{H}_{s,m}^{f,\beta}(t)$ decreases linearly with respect to the remaining distance when x is within the range $x_c\leq x\leq x_r$ according to Case 2 of Equation (14)**Error! Reference source not found.**. Case 2 is between the non-urgent scenario (that the lane change is executed far from the target point due to the risk-adverse attitude of the drivers) and the urgent lane-changing scenario (that the vehicle is so close to the target point that the lane change has to be executed). Both Case 1 and Case 2 were devised to model the minimum gap acceptance criterion of RHVs in line with Pan et al. (2016). Therefore, the response time is $\Delta T_{D,s}=\Delta T_{RHV}$. In addition, because RHVs cannot identify whether the vehicle behind it on the target lane is an RHV or a CAV, $\Delta T_{D,f}=\Delta T_{RHV}$ is adopted from the point of view of safety. Case 3 involves the urgent lane-changing demand, i.e., $x < x_c$, proposed by RHVs and the lane-changing demand proposed by CAVs. Case 3 involves the urgent MLC demand, i.e., $x < x_c$, proposed by RHVs or CAVs. For DLC

[3] The remaining distance x is defined as the distance from the current position of the subject vehicle to its target turning point. x_c and x_r denote the remaining distances by which the test section is partitioned as remote, median, and close sections, respectively, with each section corresponding to a specific level of mandatory lane-changing (MLC) urgency and minimum acceptance criterion. Taking a vehicle intending to execute an MLC as an example, the target turning point is considered to be remote as long as the remaining distance $x > x_r$ and close if $x < x_c$. In Pan et al. (2016), x_c and x_r were calibrated to be 0.05 miles and 1 mile, respectively, in their empirical study.

intention which only can be proposed by RHVs, the $H_{DLC,s,m}^{f,\beta}(t)$ is simplified as below:

$$H_{DLC,s,m}^{f,\beta}(t) \geq \tilde{H}_{DLC,s,m}^{f,\beta}(t) = \left[\underbrace{v_\beta(t)\Delta T_{RHV,f}}_{item\,1} + \underbrace{v_m(t)\Delta T_{RHV,s}}_{item\,2} + \underbrace{\frac{\left(v_\beta(t)-v_m(t)\right)^2}{2a}}_{item\,3} \right] + \underbrace{(2l+2C)}_{item\,4}$$

since an RHV cannot identify the vehicle class of the following vehicle on the target lane. Whether the target lane could provide sufficient space headway to fulfill the minimum space headway criteria is a prerequisite of a successful lane-changing maneuver. However, the final execution of a lane-changing maneuver still needs to fulfill other supplementary conditions apart from this minimum space headway criteria. This issue will be further discussed in the next section.

In summary, compared with traffic of pure RHVs, traffic flow mixed with CAVs would introduce the following three advantages: 1) the higher penetration rate of CAVs induces a higher capacity for the same freeway; 2) the minimum space headway gap required by the CAVs is smaller than that required by RHVs, for both MLC and DLC lane changing intentions; 3) the space headway in front of RHVs can be significantly enhanced if more CAVs are traveling on the segment under the same traffic conditions because CAVs tolerate a smaller headway, as illustrated in Figure 5. As it can be inferred from advantage 2) and 3), lane changing will be easier and safer.

3. Traffic-state propagation

3.1. Cell-lane representation of the multiclass traffic flow conservation

Consider a multilane freeway segment divided into several cell packages, from cell package 1 to package *N*, along the longitudinal dimension, as shown in Figure 7. Each cell package includes two cells located on lane *m* and lane *β*, denoted as cell (*i*, *m*) and cell (*i*, *β*), respectively. In this paper, we assume that there is only one bottleneck (caused by lane drop or traffic accident) on this freeway segment, which is located at the end of cell (*N*, *m*). Based on flow conservation, the cell densities $\rho_{i,m,CAV}(k+1)$ (P.C.U./mile/lane) of CAVs and $\rho_{i,m,RHV}(k+1)$ (P.C.U./mile/lane) of RHVs are respectively:

$$\begin{cases} \rho_{i,m,CAV}(k+1) = \rho_{i,m,CAV}(k) + \dfrac{T_s}{l_i}\left(q_{st,i-1,m,CAV}^{i,m}(k) + q_{i-1,\beta,CAV}^{i,m}(k)\right) - \dfrac{T_s}{l_i}\left(q_{st,i,m,CAV}^{i+1,m}(k) + q_{i,m,CAV}^{i+1,\beta}(k)\right) \\ \rho_{i,m,RHV}(k+1) = \rho_{i,m,RHV}(k) + \dfrac{T_s}{l_i}\left(q_{st,i-1,m,RHV}^{i,m}(k) + q_{M,i-1,\beta,RHV}^{i,m}(k) + q_{D,i-1,\beta,RHV}^{i,m}(k)\right) \\ \qquad - \dfrac{T_s}{l_i}\left(q_{st,i,m,RHV}^{i+1,m}(k) + q_{M,i,m,RHV}^{i+1,\beta}(k) + q_{D,i,m,RHV}^{i+1,\beta}(k)\right) \end{cases} \tag{15}$$

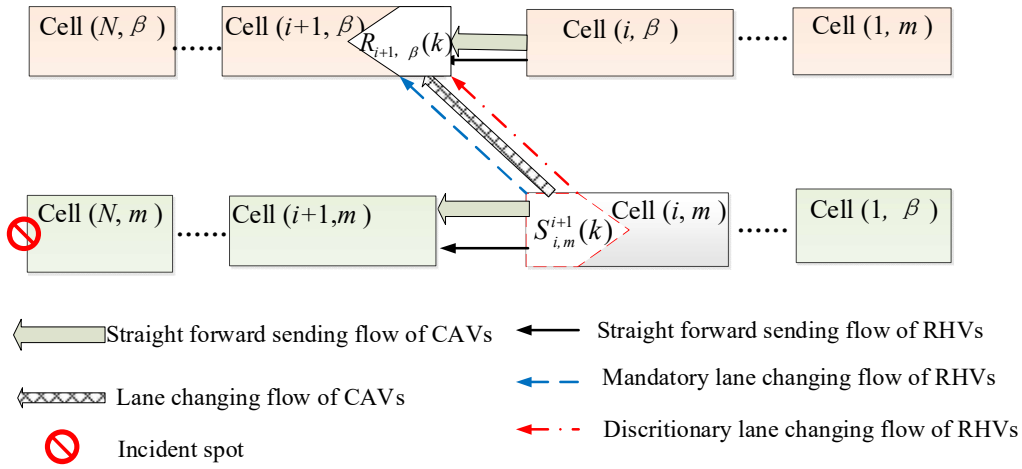

Figure 7 Merging and diverging induced by lane-changing demands of CAVs and RHVs

The cell density is a summation of the two vehicle classes, *i.e.*,

$$\rho_{i,m}(k+1)=\rho_{i,m,CAV}(k+1)+\rho_{i,m,RHV}(k+1) \tag{16}$$

whereas the proportion of CAVs in a particular cell-lane unit is given by

$$P_{i,m,\ CAV}(k+1)=\rho_{i,m,CAV}(k+1)/\rho_{i,m}(k+1) \quad if \quad \rho_{i,m}(k+1)>0$$

According to Equation (3), the cell-lane speed is given by

$$v_{i,m}(k+1)=\begin{cases}\hat{v}_{i,m}(K), & if\ \rho_{i,m}(k+1)\le\rho_{c,i,m}(k)\\ \dfrac{\left(1-l\cdot\rho_{i,m}(k+1)-C\cdot\rho_{i,m}(k+1)\right)}{\rho_{i,m}(k+1)\left(P_{i,m,CAV}(k+1)\ \Delta T_{CAV}\ +\left(1-P_{i,m,CAV}(k+1)\right)\Delta T_{RHV}\right)}, & if\ \rho_{i,m}(k+1)>\rho_{c,i,m}(k)\end{cases} \tag{17}$$

depending on whether the speed limit control or the posted **permanent compulsory** speed limit is implemented.

3.2. Sending and receiving functions for multiclass multilane traffic flow propagation

The sending and receiving functions for mixed traffic flow are extended from those developed by Pan et al. (2016) according to the new fundamental diagrams for multiclass traffic flow with various proportions of CAVs. First, the sending function $s_{i,m,D}^{i+1}(k)$ (P.C.U./hour/lane) that determines the traffic flow that intends to leave cell (*i*, *m*) for vehicle class *D* is defined as

$$s_{i,m,D}^{i+1}(k)=\begin{cases}\hat{v}_{i,m}(K)\rho_{i,m}(k)P_{i,m,D}(k) & if\ \ \rho_{i,m}(k)<\rho_{i,m,c}(k) \quad \text{for } i=1,2,\cdots N-1\\ Q_{i,m}(k)P_{i,m,D}(k) & if\ \ \rho_{i,m}(k)\ge\rho_{i,m,c}(k) \quad \text{for } i=1,2,\cdots N-1\\ S_{0,m}(k)P_{0,m,D}(k)+W_{m,\ D}(k) & \text{for } i=0\end{cases} \tag{18}$$

where $P_{i,m,D}(k)$ is the proportions of CAVs and RHVs in cell (*i*, *m*), with *D* = *CAV* and *RHV*, respectively, and

$$P_{i,m,RHV}(k)=1-P_{i,m,CAV}(k)$$

where $P_{0,m,D}(k)$ is the proportion of vehicle class D arriving at the upstream boundary, $S_{0,m}(k)$ is the demand toward lane m and $W_{m,D}(k)$ is the number of vehicles of class D queuing at the upstream boundary to cell (1, m) at simulation time step k.

The sending function $s_{i,m,D}^{i+1}(k)$ intended to leave cell (i, m) during time step k would move to the downstream cell package (i +1) involving all possible lanes, i.e., cell (i+1, β) in the adjacent lane and cell (i+1, m) in the current lane. There would be three possible lane-changing intentions: a) $s_{i,m,CAV}^{i+1,\beta}(k)$ the amount of CAVs following the lane-changing instructions issued by the VACS; b) $s_{M,i,m,RHV}^{i+1,\beta}(k)$ the amount of RHVs making MLC decisions based on lane-changing suggestions; and c) $s_{D,i,m,RHV}^{i+1,\beta}(k)$ the RHVs making DLC decisions to increase speed. These lane-changing flows can be evaluated as

$$\begin{aligned} s_{i,m,CAV}^{i+1,\beta}(k) &= s_{i,m,CAV}^{i+1}(k)\cdot \hat{p}_{i,m,CAV}^{i+1,\beta}(K) \\ s_{M,i,m,RHV}^{i+1,\beta}(k) &= s_{i,m,RHV}^{i+1}(k)\cdot p_{M,i,m,RHV}^{i+1,\beta}(k)\cdot \hat{B}_m^{\beta}(K) \\ s_{D,i,m,RHV}^{i+1,\beta}(k) &= s_{i,m,RHV}^{i+1}(k)\cdot p_{D,i,m,RHV}^{i+1,\beta}(k)\cdot\left(1-\hat{B}_m^{\beta}(K)\right) \end{aligned} \tag{19}$$

A definition constraint $0\le \hat{p}_{i,m,CAV}^{i+1,\beta}(K)\le 1$ is imposed on the proportion of CAVs issued with the MLC control. The other two proportions $p_{M,i,m,RHV}^{i+1,\beta}(k)$ and $p_{D,i,m,RHV}^{i+1,\beta}(k)$ are associated with RHVs based on human drivers' individual decisions. Once the incident alarm is disseminated through the VMS gantries, i.e., $\hat{B}_m^{\beta}(K)=1$, the MLC motivations of RHVs are triggered; otherwise, $\hat{B}_m^{\beta}(K)=0$. The term $p_{M,i,m,RHV}^{i+1,\beta}(k)$ depends on the following elements: the remaining distance x_i from the current cell package i to the incident spot, the cell density $\rho_{i,\beta}(k)$, the total MLC demand that intends to switch from lane m to lane β, $S_{M,m,RHV}^{\beta}(k)$, and the accumulation of executed MLC flow, $q_{M,j,m,RHV}^{j+1,\beta}(k)$, from cell (1, m) to cell (i, m).

$$p_{M,i,m,RHV}^{i+1,\beta}(k)=\left[S_{M,m,RHV}^{\beta}(k)\cdot \mathrm{e}^{-(x_i-x_c)^2/(\alpha_1+\alpha_2\cdot\rho_{i,\beta}(k))^2}-\sum_{j=1}^{i-1} q_{M,j,m,RHV}^{j+1,\beta}(k)\right]/\, s_{i,m,RHV}^{i+1}(k) \tag{20}$$

Interested readers are referred to Pan et al. (2016) for a detailed discussion on the detailed discussion on mandatory lane changing and the calibration of parameters α_1, α_2 and the critical remaining distance x_c (also refer to footnote No. 3 on Page 13 of this paper).

DLC (for RHVs) is motivated by the speed advantage of the adjacent lane if there is no LCR is issued to the current segment on the current lane, i.e., $\hat{B}_m^{\beta}(K)=0$.

$$p_{D,i,m,RHV}^{i+1,\beta}(k)=\frac{\max\left(0,v_{i,\beta}(k)-v_{i,m}(k)\right)}{v_f\tau} \tag{21}$$

The term τ can be interpreted as the average time a driver takes to decide and execute a lane change when the original lane is stopped, and the target lane is free-flowing (Laval and Daganzo, 2006).

Finally, the straightforward flow intended to leave cell (i, m) and enter cell (i+1, m) is

$$\begin{aligned} s_{st,i,m,CAV}^{i+1,m}(k)&=s_{i,m,CAV}^{i+1}(k)-s_{i,m,CAV}^{i+1,\beta}(k)\\ s_{st,i,m,RHV}^{i+1,m}(k)&=s_{i,m,RHV}^{i+1}(k)-s_{M,i,m,RHV}^{i+1,\beta}(k)-s_{D,i,m,RHV}^{i+1,\beta}(k)\end{aligned} \tag{22}$$

However, the final execution of all the lane changing demands and straightforward demands still depends on two external factors: the fulfillment to minimum gap acceptance criteria by target lane, and the accommodation of several merging demands considering specific priorities.

3.3. Allocation of available space for merging flows

The available space of the target cell (i+1, β) $R_{i+1,\beta}(k)$ (P.C.U./hour/lane) can be evaluated according to the fundamental diagram.

$$R_{i+1,\beta}(k)=\begin{cases} w_{i+1,\beta}(k)\left(\rho_{J,i+1,\beta}(k)-\rho_{i+1,\beta}(k)\right) & if\ \ \rho_{i+1,\beta}(k)<\rho_{c,i+1,\beta}(k)\ \ \text{for } i=0,2,\cdots N-1\\ Q_{i+1,\beta}(k) & if\ \ \rho_{i+1,\beta}(k)\geq\rho_{c,i+1,\beta}(k)\ \ \text{for } i=0,2,\cdots N-1\\ R_{E,\beta}(k) & \text{for } i=N\end{cases} \tag{23}$$

where E denotes the downstream sink connected to the last cell N.

Toward the target cell (i+1,β), there are five sending flows, i.e., $s_{st,i,m,CAV}^{i+1,m}(k)$, $s_{st,i,m,RHV}^{i+1,m}(k)$, $s_{i,m,CAV}^{i+1,\beta}(k)$, $s_{M,i,m,RHV}^{i+1,\beta}(k)$, and $s_{D,i,m,RHV}^{i+1,\beta}(k)$, where the last three elements correspond to the three minimum space headway criteria $\tilde{H}_{i,m,CAV}^{i+1,\beta}(k)$, $\tilde{H}_{M,i,m,RHV}^{i+1,\beta}(k)$, and $\tilde{H}_{D,i,m,RHV}^{i+1,\beta}(k)$. Considering the limited available space provided by the target cell, the flows that can be received by the target cell are calculated by Equations (24) and (25).

$$q_{lc,i,m,D}^{i+1,\beta}(k)=\begin{cases} s_{lc,i,m,D}^{i+1,\beta}(k) & if\ \ U_i^{i+1,\beta}(k)\leq R_{i+1,\beta}(k)\ and\ \tilde{H}_{lc,i,m,D}^{i+1,\beta}(k)\leq H_{i+1,\beta,RHV}(k)\\ \dfrac{s_{lc,i,m,D}^{i+1,\beta}(k)}{U_i^{i+1,\beta}(k)}R_{i+1,\beta}(k) & if\ \ U_i^{i+1,\beta}(k)>R_{i+1,\beta}(k)\ and\ \tilde{H}_{lc,i,m,D}^{i+1,\beta}(k)\leq H_{i+1,\beta,RHV}(k)\\ 0 & if\ \ \tilde{H}_{lc,i,m,D}^{i+1,\beta}(k)>H_{i+1,\beta,RHV}(k)\end{cases} \tag{24}$$

$$q_{st,i,\beta,D}^{i+1,\beta}(k)=\begin{cases} s_{st,i,\beta,D}^{i+1,\beta}(k) & if\ \ U_i^{i+1,\beta}(k)\le R_{i+1,\beta}(k) \\ \dfrac{s_{st,i,\beta,D}^{i+1,\beta}(k)}{U_i^{i+1,\beta}(k)}R_{i+1,\beta}(k) & if\ \ U_i^{i+1,\beta}(k)> R_{i+1,\beta}(k) \end{cases} \tag{25}$$

The subscript lc in $q_{lc,i,m,D}^{i+1,\beta}(k)$ (P.C.U./hour/lane) refers to the lane-changing motivations and D refers to vehicle class. $U_i^{i+1,\beta}(k)$ (P.C.U./hour/lane) denotes the total space required by the lane-changing demand (by fulfilling the minimum space headway criterion in the target lane) toward cell $(i+1, \beta)$.

$$U_i^{i+1,\beta}(k)=s_{st,i,\beta,CAV}^{i+1,\beta}(k)+s_{st,i,\beta,RHV}^{i+1,\beta}(k)+\sum_{lc=M}^{D}\sum_{D=\mathrm{CAV}}^{RHV}s_{lc,i,m,D}^{i+1,\beta}(k)\frac{\tilde{H}_{lc,i,m,D}^{i+1,\beta}(k)}{l},\ \ \forall \tilde{H}_{lc,i,m,D}^{i+1,\beta}(k)<H_{i+1,\beta,RHV}(k) \tag{26}$$

Based on the result of Equations (24-26), the cell densities $\rho_{i,m,CAV}(k+1)$ (P.C.U./hour/lane) of CAVs and $\rho_{i,m,RHV}(k+1)$ (P.C.U./hour/lane) of RHVs are evaluated according to Equation (15). Figure 8 presents a precedence diagram that summarizes the concept and the interconnection of different components for a better grasp and understanding of the proposed model.

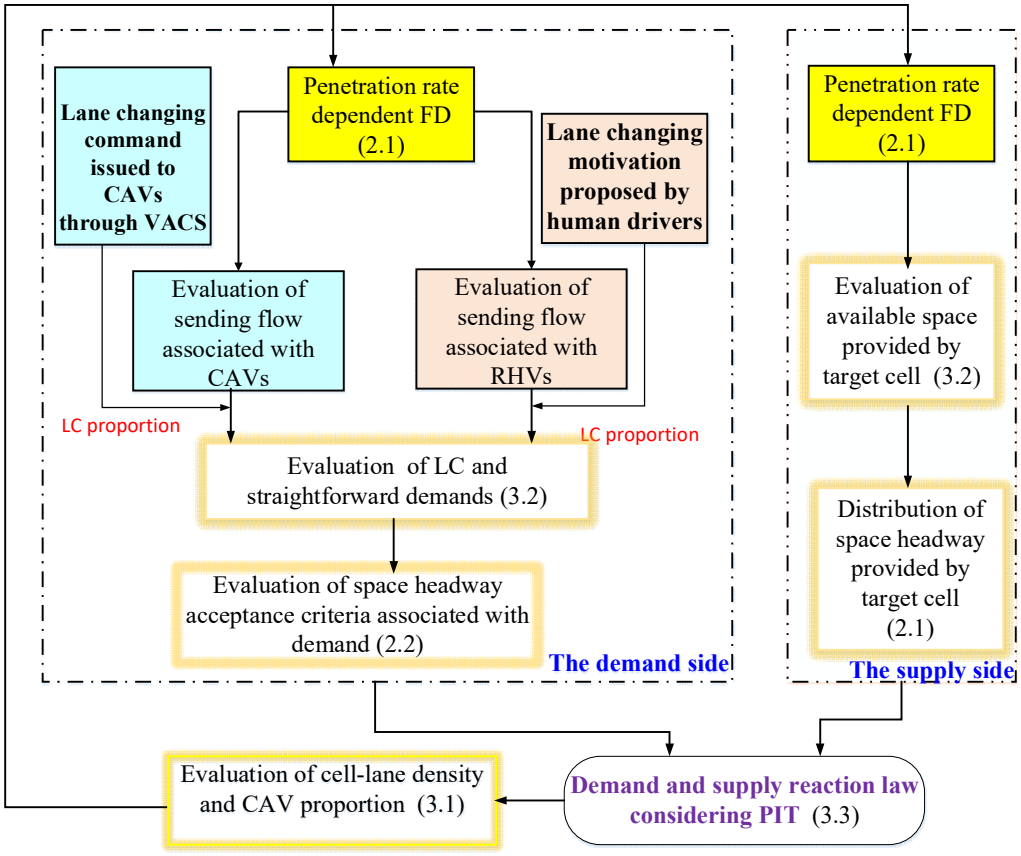

Figure 8. A precedence diagram of the model

4. Numerical simulation

The proposed model is to simulate the multiclass multilane traffic mixed with CAVs and RHVs. Unfortunately, there is no existing data recording the traffic flow characteristics of the CAVs and RHVs. Therefore, in this section, we explore the properties of the proposed model by numerical simulations, e.g., showing the effects of CAVs on traffic flow characteristics such as speed, operational capacity, fundamental diagram, total delay under different penetration rates of CAVs.

4.1. Description of the "test site"

We consider a virtual 2.75-mile-long freeway segment with two lanes as shown in Figure 9 in this numerical example. The freeway segment is without on/off-ramps. There are sufficient V2X infrastructures transmitting real-time traffic data and issuing control actions such as lane-changing controls (LCCs) and variable speed limit controls (VSLCs) to CAVs along the freeway section. Assuming that the initial time for this simulation is 0, five minutes after that, cell (11,1) is temporarily closed due to a traffic incident. Only cell (11, 2) is available for traffic, and a temporary bottleneck is thus formed. The lane closure lasts 20 min until the incident is removed. The simulation continues another 20 min to dissolve the queue afterward. In order to maintain the same total throughput with entry flow, the inflow demand is set to be 0 at the final 5 minutes. The simulation time step is 10 sec. To meet the numerical stability requirement, i.e., the Courant–Friedrichs–Lewy (CFL) condition of the CTM, the cell length should be greater than or equal to the distance traveled during a simulation time step at the free-flow speed. Therefore, this 2.75-mile-long freeway segment is divided into 11 cell packages with equal lengths of 0.25 miles.

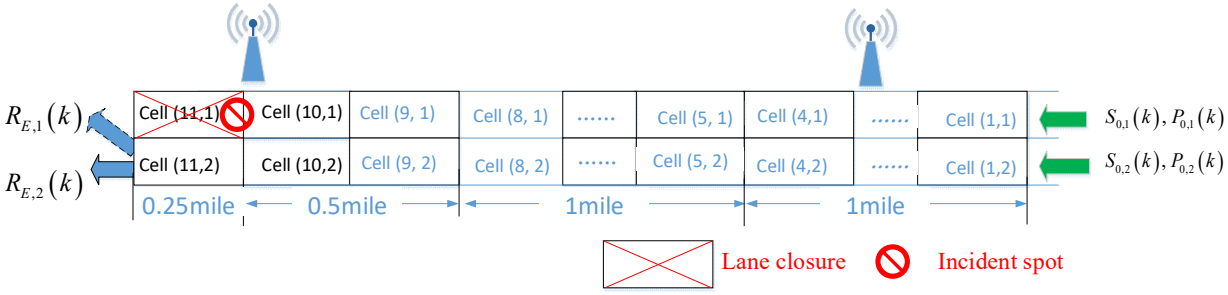

Figure 9. Topology of the "test site"

All vehicles are assumed to be P.C.U. 20 ft (6 m) long, and the safe constant gap is 6.5 ft (2 m; see the empirical study in Pan et al. (2016)). In this example, the response time is set to 1.85 sec for RHVs and 0.35 sec for CAVs[4]. The time-dependent fundamental diagram and minimum space headway acceptance criteria are then determined according to these settings. It is assumed that the

[4] Note that the response time of CAVs is assumed to vary from 0.25 sec to 1.5 sec in Levin and Boyles (2016a). The minimum headway required by CAVs is about 0.6 sec if the response time is chosen as 0.35 sec. Since the minimum headway required by CAVs would heavily affect the capacity of the freeway with mixed traffic of RHVs and CAVs, we will conduct a sensitivity analysis on several typical values of the response time of CAVs.

compulsory speed limit is 70 miles/hour under normal conditions. The parameters for evaluating the distribution of MLC and DLC demands are listed in Table 2. These parameters were calibrated and validated in Pan et al. (2016).

Table 2 Parameters adopted in the traffic model

Longitudinal cumulative distribution function of MLC demand	α_1	671
	α_2 Weighting associated with the density of the target lane	33.7
	x_c Critical remaining distance	0.05 miles
DLC demand determination function	τ Average lane-changing reaction time	3 s

4.2 Simulation results

To see how the presence of CAVs in the traffic stream would influence the bulk traffic flow, this numerical study tests three penetration rates of CAVs, i.e., 0% for the pure RHVs case (which is termed as Case A), 33.3% (which is termed as Case B) and 66.7% for mixed traffic case (which is termed as Case C). In the simulation setting, no LC recommendations are disseminated to RHVs. Therefore, all the drivers would make their own decisions according to their perceived traffic conditions. The CAVs traveling in the incident lane would follow the non-optimized LCCs, such as remaining in the current lane until the remaining distance to the incident spot is less than 0.2 miles. It should be noted that the CAVs are always with full automatic control. Otherwise they can be regarded as RHVs. Therefore, when we mention "without control" we mean that the control is only applied to the CAVs rather than to coordinate the movements of the RHVs and CAVs. The inflow profile is 1125 P.C.U./hour/lane.

Figure 10 depicts the spatial-temporal distribution of traffic density and speed for Case A. Before the incident occurred (0-5 min), the inflow demand is less than the freeway capacity (the nominal capacity for pure RHVs is 1719 P.C.U./hour/lane (Case A), 2294 P.C.U./hour/lane for 33.3% penetrated case (Case B), and 3446 P.C.U./hour/lane for 66.7% penetrated case (Case C)). Under normal condition (the period before the incident happened), no congestion would form under such setting, see, e.g., Figure 10 a). As soon as the occurrence of the incident, lane 1 is closed. Traffic demand exceeds the theoretical bottleneck capacity; congestion starts to onset. As the divers do not know about the incident until they reach the incident spot or join the queue, the queue on lane 1 quickly spills upstream after the lane closure (as it can be inferred from Figure 10 a). After they reach the tail of the queue, they have to switch to lane 2 due to the lane blockage. As it can be observed from Figure 10 a), when the vehicles join the queue, they would travel at a low speed and seek for a chance to execute an MLC. When an MLC maneuver is executed by such a vehicle with low speed, the speed in lane 2 is also brought down. As a consequence, density on lane 2 increases thus causing congestion in lane 2. As revealed in the literature, this kind of speed reduction causes by the lane-changing maneuvers can further induce the capacity drop, i.e., the capacity at the bottleneck is much lower than the theoretical value, especially when the lane-changing flow ratio is large, see e.g., Pan et al. (2016); Zhang and Ioannou (2017) and the references therein). With the penetration of CAVs, traffic congestion becomes less severe, see, e.g., Figure 10 b) and c), because autonomous driving can achieve a faster lane changing execution and require a smaller minimum safety gap. However,

when the penetration rate is not high (i.e., Case B), the effect is limited. In contrast with Figure 10 b), the congestion alleviation is evident under the high penetration rate case, i.e., Case C in Figure 10 c). However, the congestion cannot be well resolved by autonomous driving only (especially when the penetration rate of CAVs is low) as indicated in Figure 10 and Table 3.

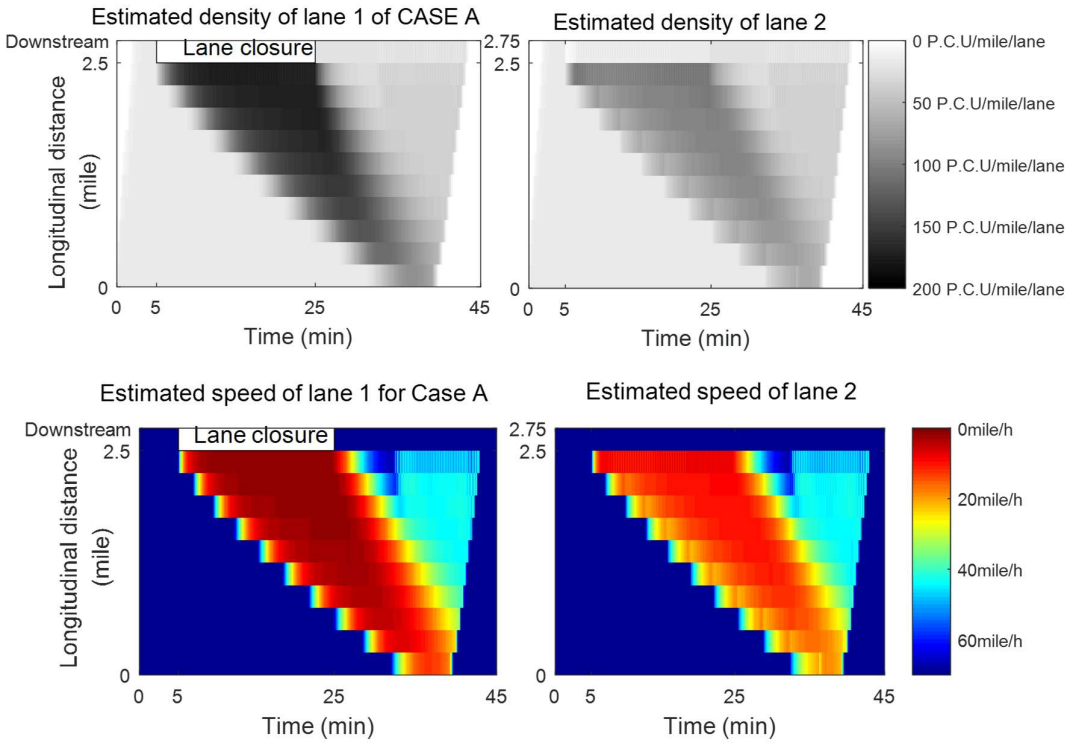

a) Case A1 (0% penetration rate with 1125 P.C.U./hour/lane inflow demand)

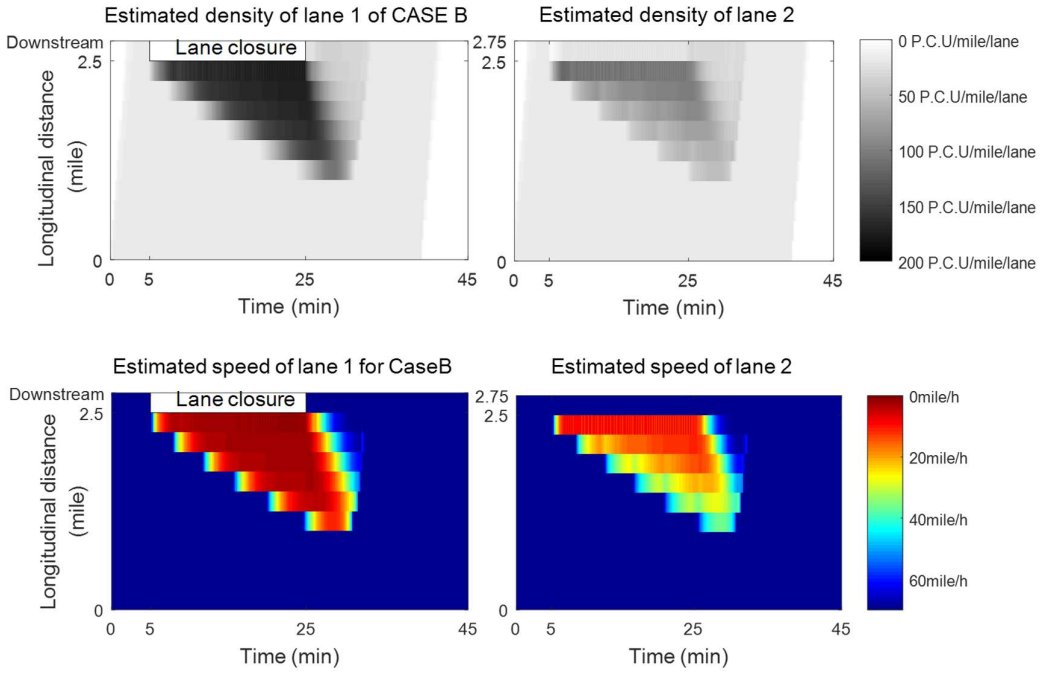

b) Case B1 (33.3% penetration rate with 1125 P.C.U./hour/lane inflow demand)

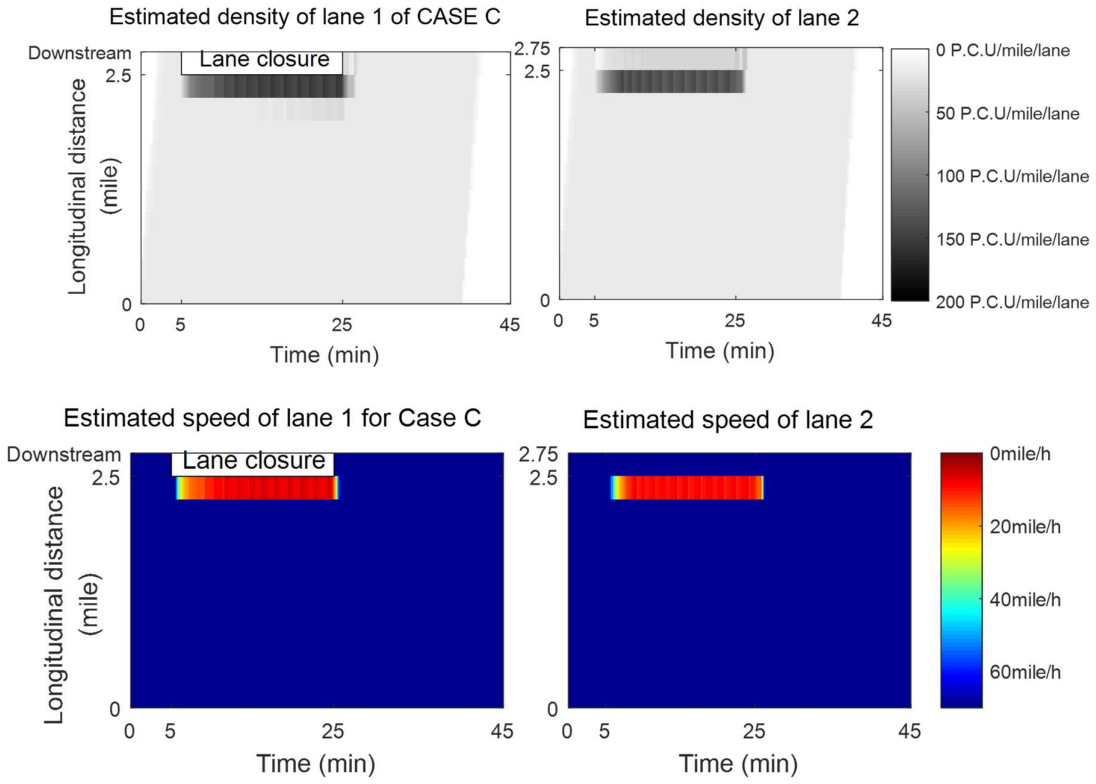

c) Case C1 (66.7% penetration rate with 1125 P.C.U./hour/lane inflow demand)

Figure 10. Spatial-temporal density and speed maps of the baseline cases penetration rate and demand (left-hand side: lane 1 (with incident); right-hand side: lane 2)

Vehicles have to slow down considerably when approaching the incident spot or the tail of the queue without being aware that their lane is blocked. Apart from a capacity drop, an **oscillation in traffic speed** of the bottleneck cell can be observed from Figure 11 for the pure RHV case (Case A). Without acknowledgment of the incident, vehicles traveling in the incident lane would change lanes only when they reach the incident spot or arrive at the tail of the queue, see, e.g., Figure 12. In either case, they have to slow down considerably to execute an MLC maneuver to the open lane. When the low-speed vehicle changes to the open lane, vehicles traveling in the open lane have to slow down to adapt to the speed of its leading vehicle (i.e., the lane-changing vehicle) to guarantee traffic safety, as shown in the solid blue line of Figure 11. The speed of the open lane would increase only if the lane-changing vehicle increases its speed. Note that the freeway is under oversaturated traffic condition, the process would keep happening if there is any MLC maneuver executed by low-speed vehicle from the closed lane. With the penetration of CAVs, such speed oscillation can be alleviated, especially when the penetration rate of CAVs is high. This is because the CAVs can achieve a faster lane changing execution while requiring a smaller minimum safety headway and can make a faster acceleration. The penetration of CAVs delays speed breakdown of the bottleneck cell as indicated in Figure 11.

On the other hand, there is the so-called "friction effect" from the empirical observation that drivers' fear of moving fast in open lanes when an incident or slowly moving vehicles exist in adjacent lanes.

As observed in Zhang and Ioannou (2017) that which forced lane changes in close proximity to the incident were the major cause of capacity drop and thus reducing the actual operational capacity of the bottleneck, as shown in Figure 13. As depicted in Figure 13 a), the operational capacity is oscillating between 950-1350 P.C.U./hour during the lane blockage period, which is lower than its nominal value (i.e., the capacity of a single lane) of 1719 P.C.U./hour when there is no lane changing flow. The operational capacity increases with respect to the penetration rate of CAVs. At the meanwhile, the oscillation of operational capacity becomes weaker when the penetration rate of CAVs becomes higher. With fewer interruptions caused by lane changing maneuvers, the capacity drop effect at the bottleneck can be reduced (Zhang and Ioannou, 2017). As shown in Figure 13, during 12-25 minute the average operational capacity of the bottleneck increases from 1170 (Case A) to 2230 (Case C) P.C.U./hour and the standard deviation reduces from 163 (SD/Mean ratio14%) (Case A) to 72 (SD/Mean ratio 3.2%) (Case C) P.C.U./hour.

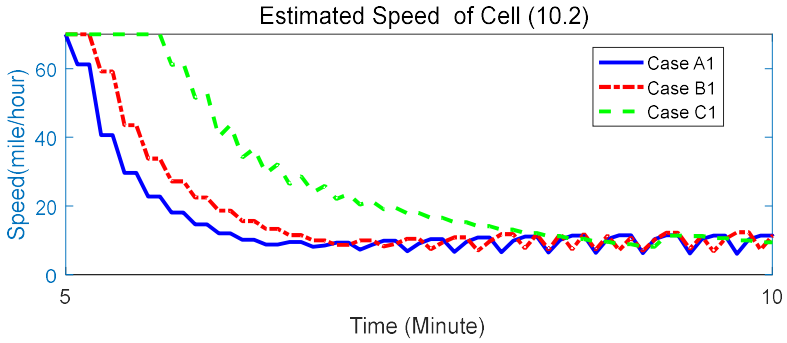

Figure 11. Speed oscillation of Cell (10,2)

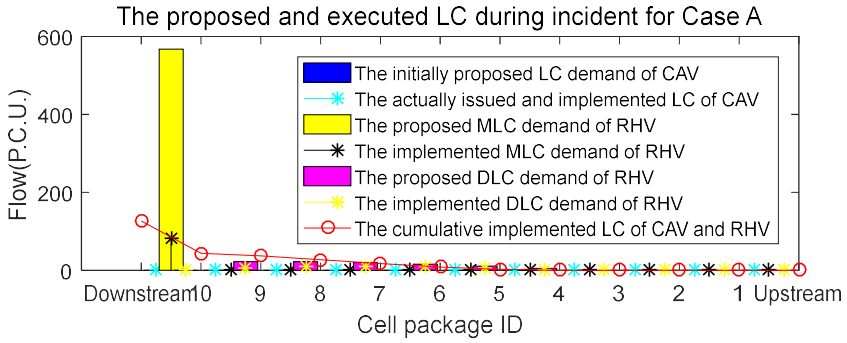

(a) Case A

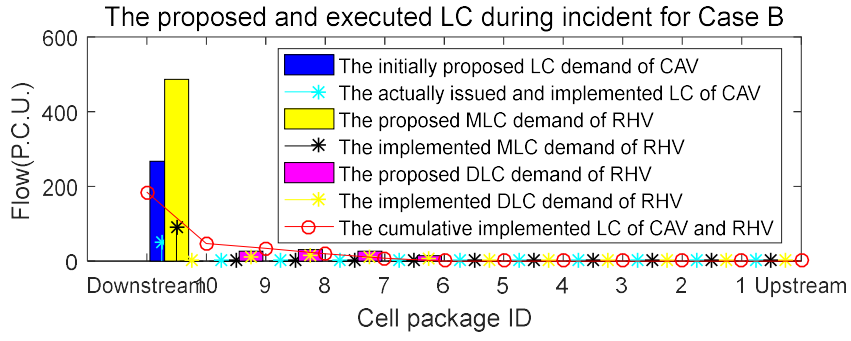

(b) Case B

Figure 12. The proposed and executed cumulative lane changing flows

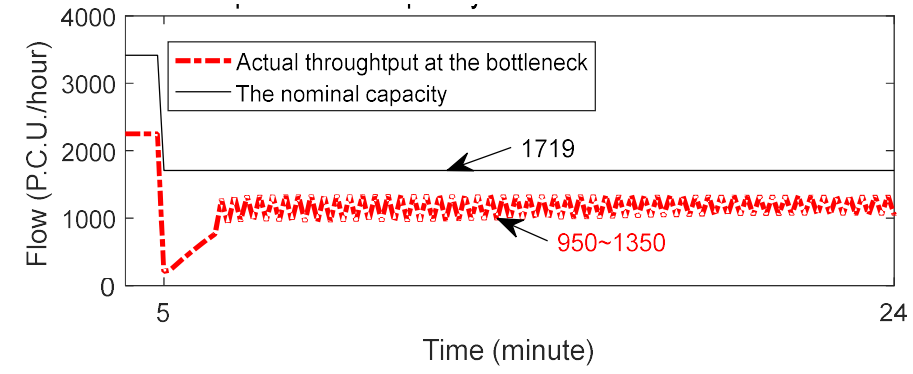

(a).Case A

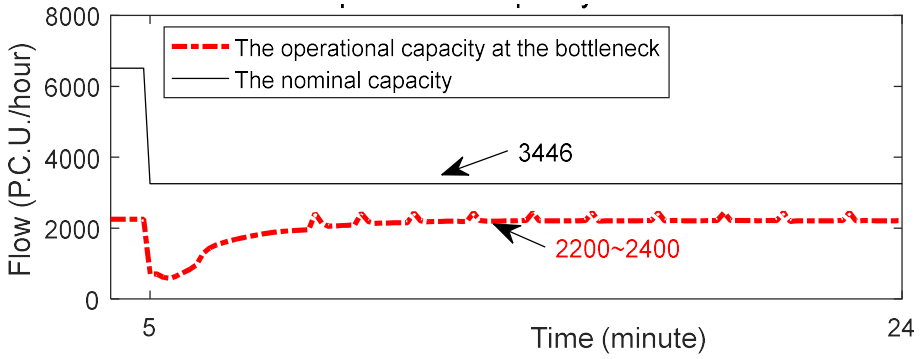

(b). Case C

Figure 13. Operational capacity during the lane blockage

Table 3. Total travel time spent and speed profile with different penetration rates of CAVs

Inflow demand (P.C.U./hour/lane)	Penetration rate	Average Speed (mile/hour)	Speed deviation	Total travel time (P.C.U. hour)	Cumulative exit flow
1125	0%	15	26.8%	189	1500
	10%	16	24.5%	167	1500
	33.3%	21	20.0%	124	1500
	66.7%	40	0.5%	74	1500
	100%	70	0%	55	1500

As previously mentioned, the penetration rate of the CAVs significantly affects the freeway operational characteristics. Sensitivity analysis is conducted to demonstrate the performance of the speed profile against the penetration rate of CAVs. Apart from the average velocity, the standard deviation of traffic velocity is a common measure to quantify the traffic state in the literature, see, e.g., Stern et al., (2017). For our concern, we are interested in the speed deviation during the incident period since the lane-changing maneuvers are the primary causes of capacity drop and traffic breakdown. Table 3 presents the (weighted) mean and deviation of the speed profile of the segment during 12-25 minute (incident period) under different penetration rates of CAVs. As indicated in the table, the presence of CAVs can significantly increase the mean speed while reducing the speed variation at the same time. When the penetration rate of CAVs is low, the improvement is not

significant (both mean and standard deviation). When the penetration rate of CAVs is high enough, the bottleneck traffic speed could be smoothed as indicated in Figure 11. This in conjunction with Figure 10 suggests that cell traffic speed can recover from abnormal traffic conditions in a much faster way when the penetration rate of CAVs is high. The advantage of CAVs in reducing total travel time is also highlighted in Table 3. With a penetration rate of 66.7% of CAVs, the total travel time can be reduced by about 60% under over-saturated traffic condition.

Table 4. The platooning and re-calibration of the capacity

Penetration rate	Size of CAVs platooning	Ratio of C-C gap	Ratio of R-C gap	Ratio of C-R and R-R gap	Re-calibration of the capacity
33.3%	1	0	1/3	2/3	1991
	3	2/9	1/9	6/9	2164
	6	5/18	1/18	12/18	2212
	9	8/27	1/27	18/27	2229
	12	11/36	1/36	24/36	2237
66.7%	2	1/3	1/3	1/3	2753
	6	5/9	1/9	3/9	3095
	8	7/12	1/12	4/12	3144
	12	11/18	1/18	6/18	3194

C-C (CAV following CAV): Response time 0.35sec
R-C (CAV following RHV): Response time 0.7sec
R-R/C-R (RHV following RHV/CAV): Response time: 1.85sec

Platooning of CAVs decreases the headway of vehicles by a cooperative adaptive cruise control (CACC) algorithm that would maintain a tight headway and thus achieve a large saturation flow rate. In this test, we investigate the effect of platooning size of CAVs by sensitivity analysis (by specifying the upstream arrival process of CAVs). It is assumed that the lane changing maneuvers of RHVs cannot interrupt the CAV platoon. There are several car following scenarios, such as CAV (leading)-CAV (following), RHV-CAV, RHV-RHV, CAV- RHV, admitting different time headway distributions. The CAV-CAV can achieve the smallest headway. For the case when a CAV follows an RHV, since the reaction time of a CAV is very small and the assumption that the CAVs have to know the position and speed of some following vehicles and the direct preceding vehicle in real time regardless whether the following and the preceding vehicles are CAVs or not through either V2X technology or their own detectors, the headway can be small too. For other two car-following cases, conventional RHV car-following headway is adopted. Therefore, we adopted the settings presented at the bottom of Table 4. Simulation results are presented in Table 4. It can be observed that the capacity will increase with the size of CAV platoon in general under the same inflow profile. The increase will not be significant when the size of the CAV platoon is already large enough, e.g., 6 CAVs for the 33.3% case and 8 CAVs for the 66.7% case. This implies that a proper platoon size of CAVs can be identified for the purpose of maximizing the capacity under the mixed RHV and CAV scenarios.

4.3 Discussion

From the above simulation analysis, we can see that the congestion cannot be well resolved by autonomous driving only especially when the penetration rate of CAVs is low. Freeway control schemes that aim to improve traffic flow efficiency are required. Through the VACS, the CAVs can adjust their driving status such as speed, lane, and headway according to the control. Zhu and Ukkusuri (2017) termed this kind of driving behavior as proactive driving behavior. Note that the proactive driving behavior can help to smooth the traffic flow and improving its performance. Literature has shown that using a CAV as the leading vehicle to influence the driving behavior of RHVs, the efficiency of traffic flow mixed with CAVs and RHVs can be significantly improved (Stern et al., 2017). An implication from these findings is that, if the prevailing traffic information is available, RHVs could also adjust their driving status such as speed according to the VSLR released by the VMS gantry rather than blindly adjust speed based on the speed change of the leading vehicle (so does the lane choice). In other words, RHVs can also drive proactively to a certain extent, although not as proactive as CAVs, e.g., Equation (20) (which is an extension of the CTM to account for the proactive driving behavior of RHVs). One promising future direction is to devise an integrated traffic control strategy including the variable speed limit (VSL) and lane-changing control (LCC) for improving the efficiency of freeway traffic mixed with RHVs and CAVs using the VACS and the en-route Variable Message Signs (VMS) under various penetration rates of CAVs. Preliminary results in Pan et al. (preprint) show that the traffic flow could be smoothed if their drivers are willing to follow the control information such as the LCR and VSLR disseminated through VMS gantry while the CAVs will follow the control through VACS.

5. Conclusions

To support the design of the freeway traffic control schemes with different market penetration of CAVs, a new multiclass multilane traffic flow model was proposed in this paper to simulate traffic flow dynamics mixed with CAVs and RHVs. This new multiclass multilane CTM-based model explicitly considers the effect of variations in headway and safety gap distributions with respect to different vehicle-class proportions within each cell on its fundamental diagram. The impact of the implemented speed limit control on the fundamental diagram is also explicitly considered in the proposed model. Meanwhile, different safety gap acceptance criteria were proposed to consider various lane-changing maneuvers of different vehicle types (RHVs and CAVs) with different lane-changing intentions to guarantee traffic safety and lane-changing priorities. The proposed model includes driver's anticipation on lane choice regarding the headway, acceleration, and their distance to the target location. It was found by numerical investigation that the proactive driving of CAVs can smooth traffic flow resulting in an improvement on average traffic speed while reducing traffic speed oscillation. Substantial potential operational capacity increases are possible under certain market penetration scenarios. The advantage of CAVs in reducing total travel cost is highlighted in the numerical example. Further study is recommended to extend the proposed framework for empirical experiments under controlled environments such as Stern et al. (2017) and to develop an optimal control framework that integrates several traffic control schemes for improving the efficiency of freeways.

Acknowledgments

The work described in this paper was jointly supported by a Postgraduate Studentship of the Hong Kong Polytechnic University, the Research Grants Council of the Hong Kong Special Administrative Region, China (Project No. PolyU 152074/14E) and the Research Institute for Sustainable Urban Development (RISUD) of the Hong Kong Polytechnic University (Project Nos. 1-ZVBY and 1-ZVBZ).

References

1. van Arem, B., van Driel, C., and R. Visser, 2006. The Impact of Cooperative Adaptive Cruise Control on Traffic-Flow Characteristics. IEEE Transactions on Intelligent Transportation Systems, 7(4), 429–436.
2. Bekiaris-Liberis, N., Roncoli, C., Papageorgiou, M., 2016. Highway traffic state estimation with mixed connected and conventional vehicles. IEEE Transactions on Intelligent Transportation Systems, 17(12), 3484-3497.
3. Chen, D., Ahn, S., Chitturi, M., and Noyce, D. 2017. Towards vehicle automation: Roadway capacity formulation for traffic mixed with regular and automated vehicles. Transportation Research Part B, 100, 196-221.
4. Diakaki, C., Papageorgiou, M., Papamichail, I., Nikolos, I., 2015. Overview and analysis of vehicle automation and communication systems from a motorway traffic management perspective. Transportation Research Part A, 75, 147-165.
5. Fountoulakis, M., Bekiaris-Liberis, N., Roncoli, C., Papamichail, I., and Papageorgiou, M., 2017. Highway traffic state estimation with mixed connected and conventional vehicles: Microscopic simulation-based testing, Transportation Research Part C, 78, 13-33.
6. Green, M., 2000. "How long does it take to stop?" methodological analysis of driver perception -brake times. Transportation human factors, 2(3), 195-216.
7. Hall, R., and C. Chin, 2005. Vehicle sorting for platoon formation: Impacts on highway entry and throughput. Transportation Research Part C, 13(5-6), 405–420.
8. Hegyi, A., Schutter, B., Hellendoorn, H., 2005. Model predictive control for optimal coordination of ramp metering and variable speed limits. Transportation Research Part C, 13(3), 185-209.
9. Highway Capacity Manual 2010, Transportation Research Board of the National Academy of Sciences.
10. Hidas, P., 2005. Modelling vehicle interactions in microscopic simulation of merging and weaving. Transport. Res. Part C 13 (1), 37–62.
11. Jepsen, M. On the speed-flow relationships in road traffic: a model of driver behaviour. In Proceedings of the Third International Symposium on Highway Capacity. 1998.
12. Khondaker, B., Kattan, L., 2015. Variable speed limit: A microscopic analysis in a connected vehicle environment. Transportation Research Part C, 58, 146-159.
13. Lerner, M, Huey, R., Mcgee, H., and Sullivan. A (1995). Older driver perception reaction time for intersection sight distance and object detection, 1(1995), 33-40. Report FHWA-RD-93-168, Federal Highway Administration, US-DOT, Mclean, Virginia.
14. Levin, M., and Boyles, S., 2016a. A multiclass cell transmission model for shared human and autonomous vehicle roads. Transportation Research Part C, 62, 103-106.

15. Levin, M., and Boyles, S., 2016b. A cell transmission model for dynamic lane reversal with autonomous vehicles. Transportation Research Part C, 68 126-143.
16. Milanes, V., Shladover, S.E., 2014. Modeling cooperative and autonomous adaptive cruise control dynamic responses using experimental data. Transportation Research Part C, 48, 285–300.
17. Milanes, V., Shladover, S., Spring, J., Nowakowski, C., Kawazoe, H., Nakamura, M., 2014. Cooperative adaptive cruise control in real traffic situations. IEEE Transactions on Intelligent Transportation Systems, 15, 296–305.
18. Pan, T., Lam, W.H.K., Sumalee, A., Zhong, R., 2016. Modelling the impacts of mandatory and discretionary lane-changing maneuvers. Transportation Research Part C, 68, 403-424.
19. Pan, T., Lam, W.H.K., Sumalee, A., Zhong, R., preprint. Optimal control strategies for freeway traffic mixed with connected automated vehicles.
20. Roncoli, C., Papageorgiou, M., Papamichail, I., 2015. Traffic flow optimisation in presence of vehicle automation and communication systems – Part I: a first-order multi-lane model for motorway traffic. Transportation Research Part C, 57, 241–259.
21. Wang, M., Daamen, W., Hoogendoorn, S.P., van Arem, B., 2016a. Connected variable speed limits control and car-following control with vehicle-infrastructure communication to resolve stop-and-go waves. Journal of Intelligent Transportation Systems, DOI: 10.1080/15472450.2016.1157022.
22. Wang, M., Daamen, W., Hoogendoorn, S.P., van Arem, B., 2016b. Cooperative car-following control: Distributed algorithm and impact on moving jam features. IEEE Transactions on Intelligent Transportation Systems. 17(5), 1459-1471.
23. Wang, R., Li, Y., and Work, D. 2017. Comparing traffic state estimators for mixed human and automated traffic flows. Transportation Research Part C, 28, 95-110.
24. Wierwille,W., Casali, J., 1983. Driver steering reaction time to abrupt-onset human factors, 1983, 2(1), 103-116.
25. Zhang, Y., and Ioannou, P., 2017. Combined variable speed limit and lane change control for highway traffic. IEEE Transactions on Intelligent Transportation Systems, 18 (7), 1812 - 1823.
26. Zhu, F., Ukkusuri, S., 2017a. Modeling the proactive driving behavior of connected vehicles: A cell-based simulation approach. Computer-Aided Civil and Infrastructure Engineering, inpress.
27. Zhu, F., Ukkusuri, S., 2017b. An optimal estimation approach for the calibration of the car-following behavior of connected vehicles in a mixed traffic environment. IEEE Transactions on Intelligent Transportation Systems, 18(2), 282-291.
28. Zhou, M., Qu, X., Jin, S., 2017. On the impact of cooperative autonomous vehicles in improving freeway merging: a modified intelligent driver model-based approach. IEEE Transactions on Intelligent Transportation Systems, 18 (6), 1422-1428.
29. Ngoduy, D., Jia, D., 2017. Multi anticipative bidirectional macroscopic traffic model considering cooperative driving strategy. Transportmetrica B, 5 (1), 96-110.
30. Jia, D., Ngoduy, D., 2016a. Enhanced cooperative car-following traffic model with the combination of V2V and V2I communication. Transportation Research Part B, 90, 172–191.
31. Jia, D., Ngoduy, D., 2016b. Platoon based cooperative driving model with consideration of realistic inter-vehicle communication. Transportation Research Part C, 68, 245–264.
32. J Jia, D., Ngoduy, D., Vu, H., inpress. A multiclass microscopic model for heterogeneous platoon with vehicle-to-vehicle communication. Transportmetrica B: Transport Dynamics, 1-25.

33. Talebpour, A., Mahmassani, H. S., 2016. Influence of connected and autonomous vehicles on traffic flow stability and throughput. Transportation Research Part C, 71, 143–163.
34. Stern, R., Cui, S., Monache, M.L., Bhadani, R., Bunting, M., Churchill, M., Hamilton, N., Haulcy, R., Pohlmann, H., Wu, F., Piccoli, B., Seibold, B., Sprinkle, J., Work, D. B., 2018. Dissipation of stop-and-go waves via control of autonomous vehicles: Field experiments. Transportation Research Part C, 89, 205–221.
35. Lioris, J., Pedarsani, R., Tascikaraoglu, F., Varaiya, P., 2017. Platoons of connected vehicles can double throughput in urban roads, Transportation Research Part C, 77, 292-305.

Appendix: Key variables of the multiclass multilane traffic flow model

Elements	Notation description
$\rho_{i,m,CAV}(k)$	Density of CAVs on cell (i, m) during step k
$\rho_{i,m,RHV}(k)$	Density of RHVs on cell (i, m) during step k
$P_{i,m,CAV}(k)$	Penetration rate of CAVs on cell (i, m) during step k
$v_{i,m}(k)$	Traffic speed on cell (i, m) during step k
$s_{i,m,CAV}^{i+1,\beta}(k)$	Sending function of lane-changing demand ordered to CAVs from cell (i, m) to cell (i+1, β) during step k
$s_{M,i,m,RHV}^{i+1,\beta}(k)$	Sending function of RHVs with MLC or DLC demand from cell (i, m) to cell (i+1, β) during step k
$s_{D,i,m,RHV}^{i+1,\beta}(k)$	
$s_{st,i,m,CAV}(k)$	Sending function of flow with vehicle class CAV or RHV that intend to leave cell (i, m) and be received by downstream cell (i + 1, m) during step k
$s_{st,i,m,RHV}(k)$	
$\tilde{H}_{i,m,CAV}^{i+1,\beta}(k)$	Minimum space headway criteria of $s_{i,m,CAV}^{i+1,\beta}(k)$
$\tilde{H}_{M,i,m,RHV}^{i+1,\beta}(k)$	Minimum space headway criteria of $s_{M,i,m,RHV}^{i+1,\beta}(k)$ and $s_{D,i,m,RHV}^{i+1,\beta}(k)$
$\tilde{H}_{D,i,m,RHV}^{i+1,\beta}(k)$	
$q_{M,i,m,CAV}^{i+1,\beta}(k)$	The amount of $s_{i,m,CAV}^{i+1,\beta}(k)$ received by the target cell
$q_{M,i,m,RHV}^{i+1,\beta}(k)$	The amount of $s_{M,i,m,RHV}^{i+1,\beta}(k)$ and $s_{D,i,m,RHV}^{i+1,\beta}(k)$ received by the target cells, respectively
$q_{D,i,m,RHV}^{i+1,\beta}(k)$	
$q_{st,i,m,CAV}(k)$	The amount of $s_{st,i,m,CAV}(k)$ and $s_{st,i,m,RHV}(k)$ received by the target cells
$q_{st,i,m,RHV}(k)$	
$R_{i,m}(k)$	Receiving function of cell (i, m) during step k
$\hat{v}_{i,m,l}(K)$	Implemented speed limit on cell (i, m) during control cycle K
$\hat{p}_{i,m,CAV}^{i+1,\beta}(K)$	Proportion of CAVs that are issued to switch from cell (i, m) to cell (i+1, β) during control cycle K

$\hat{v}_{i,m}(K)$	Speed limit control on cell (i, m) during cycle K
$\rho_{i,m,c}(k)$	Critical density on cell (i, m) at simulation step k
$Q_{i,m}(k)$	Capacity on cell (i, m) at simulation step k
$w_{i,m}(k)$	Wave-back speed on cell (i, m) at simulation step k
$\rho_{i,m,J}(k)$	Jams density on cell (i, m) at simulation step k
$S_{0,m}(k)$	Inflow demand of lane m at simulation step k
$P_{0,m,CAV}(k)$	Proportion of CAVs associated with $S_{0,m}(k)$
$R_{E,m}(k)$	Available space of downstream section at simulation step k
RHV	Regular Human-piloted Vehicle
PIT	Priority Incremental Transfer
SSL	Spontaneous Speed Limit
DLC	Discretionary Lane Changing
MLC	Mandatory Lane Changing
ISL	Implemented Speed Limit
VACS	Vehicle Automation and Communication System
VSLC	Variable Speed Limit Control
LCC	Lane Changing Control